$ar{B} ightarrow D^{(*)} \mathscr{C} ar{X}$ decays in effective field theory with massive right-handed neutrinos

Alakabha Datta⁰, ^{1,*} Hongkai Liu⁰, ^{2,†} and Danny Marfatia^{3,4,‡}

¹Department of Physics and Astronomy, University of Mississippi, Oxford, Mississippi 38677, USA

²Department of Physics, Technion - Israel Institute of Technology, Haifa 3200003, Israel

³Department of Physics and Astronomy, University of Hawaii at Manoa, Honolulu, Hawaii 96822, USA

⁴Kavli Institute for Theoretical Physics, University of California, Santa Barbara, California 93106, USA

(Received 8 April 2022; accepted 18 July 2022; published 28 July 2022)

We calculate the complete differential decay distributions for the B meson decays, $\bar{B} \to D^{(*)}\ell\bar{X}$, to a massive right-handed (RH) neutrino in the low-energy effective field theory (LEFT) framework. We find that a massive RH neutrino does not introduce any new angular structures compared to the massless case, but can cause significant distortions in angular observables. We study the phenomenology of low-energy four-fermion operators permitted by the standard model effective field theory (SMEFT) extended with RH neutrinos (SMNEFT). We show that to explain the positive value of the difference in forward-backward asymmetries, $\Delta A_{\rm FB} \equiv A_{\rm FB}^{\mu} - A_{\rm FB}^{e}$, tentatively inferred from Belle data, the RH neutrino must be massive. We also make predictions for q^2 dependent angular observables to motivate future measurements.

DOI: 10.1103/PhysRevD.106.L011702

I. INTRODUCTION

Hints of new physics (NP) have been reported in the charged current decays, $B \to D^{(*)} \tau \nu_{\tau}$, by the BABAR, Belle and LHCb experiments. Measurements of the ratios, $R_{D^{(*)}}^{\tau/\ell} \equiv \mathcal{B}(\bar{B} \to D^{(*)} \tau^- \bar{\nu}_{\tau})/\mathcal{B}(\bar{B} \to D^{(*)} \ell^- \bar{\nu}_{\ell})$, where $\ell = e$, μ , are larger than the standard model (SM) predictions [1–10] with a combined significance of 3.4σ [11]. This is known as the $R_{D^{(*)}}$ puzzle. Measurements of a similar ratio, $R_{J/\psi}^{\tau/\mu} \equiv \mathcal{B}(B_c^+ \to J/\psi \tau^+ \nu_\tau)/\mathcal{B}(B_c^+ \to J/\psi \mu^+ \nu_\mu)$ [12], also show tension with the SM at 1.7σ significance [13]. These measurements suggest NP in $b \to c\tau^- \bar{\nu}$ decays that is lepton universality violating (LUV).

Not surprisingly, most of the theoretical work on NP has been concentrated on semileptonic τ modes with a left-handed (LH) neutrino in the final state. If NP allows for decays to a light right-handed (RH) neutrino, the decay rate is always enhanced because there is no interference with the SM amplitude in the limit of vanishing active neutrino mass. This feature can be used to naturally explain the $R_{D^*}^{\tau/\ell}$ measurements [14–19]. However, with the limited

Published by the American Physical Society under the terms of the Creative Commons Attribution 4.0 International license. Further distribution of this work must maintain attribution to the author(s) and the published article's title, journal citation, and DOI. Funded by SCOAP³. experimental statistics, it is difficult to find clear signals of NP. Moreover, since the final state contains one or more additional neutrinos from τ decay, measurements of angular distributions that are crucial for detecting NP are further complicated.

In the coming years, the B factories, Belle II and LHCb, may conclusively confirm the existence of beyond the standard model (SM) physics in semileptonic B decays. In this paper, we study the high statistics charged current $\bar{B} \to D^{(*)} \ell \bar{X}$ decay arising from the underlying $b \to c \ell^- \bar{X}$ transition, where $\ell = e$, μ and the invisible state X can be a LH neutrino or a light RH singlet neutrino. At Belle II with 50 ab⁻¹ we expect 8×10^6 events in each of the muon and electron modes. These modes allow full event reconstruction because the missing neutrino momentum can be calculated from the e^+e^- kinematics at the $\Upsilon(4S)$.

New physics in the muon sector is motivated by anomalies in the measured value of $(g-2)_{\mu}$ [20] and neutral-current $b \to s \mu^+ \mu^-$ decays [21]. Since our interest is in LUV NP, we assume NP to affect only the muon sector while the electron sector is described by the SM. In this spirit we introduce a RH neutrino associated with the muon. LUV NP in the electron and muon sectors is tightly constrained by the measurement of the ratio of rates, $R_{D^{(*)}}^{\mu/e} \equiv \mathcal{B}(\bar{B} \to D^{(*)} \mu^- \bar{\nu}_{\mu})/\mathcal{B}(\bar{B} \to D^{(*)} e^- \bar{\nu}_e)$ which is within 5% of unity. We restrict ourselves to NP scenarios in which this ratio can deviate up to 3% from unity, a precision achievable in the future.

A key point is that even if the effects of LUV NP are small in the ratios of decay rates, larger effects may be visible in the angular distributions as functions of q^2 , and angular

^{*}datta@phy.olemiss.edu

liu.hongkai@campus.technion.ac.il

[‡]dmarf8@hawaii.edu

observables may provide one or more unambiguous signals for NP. One of the issues that should be addressed is whether form factor uncertainties can obscure these signals. Fortunately, we can identify two types of observables in the SM that have very little or no form factor uncertainties and hence any measured deviations from the SM predictions for these observables would be clear signs of NP. The first are the Δ observables that quantify differences in the angular observables for the muon and electron channels, e.g., $\Delta A_{\rm FB} \equiv A_{\rm FB}^{\mu} - A_{\rm FB}^{e}$, where $A_{\rm FB}$ is the forward-backward asymmetry. The second type are the CP-violating tripleproduct terms in the angular distribution [22,23] which can be nonzero if NP couplings are complex and have phases different from the SM contribution. The measurements of CP violating terms require large statistics [24], and so we focus on the Δ observables in this work. Recently, using the tables of Belle data in Ref. [25], an anomaly in $\Delta A_{\rm FR}$ was reported in Ref. [26]. If confirmed, this could signal LUV [24,26,27]. As an application of our formalism, we explore if decays to a massive RH neutrino can resolve this anomaly.

Note that while the effects of a right-handed neutrino have been considered in the τ channel, our approach has several novel features. (1) In our framework, the structure of the low energy effective operators is assumed to arise from the standard model effective field theory (SMEFT) extended with RH neutrinos (SMNEFT). Consequently, only the subset of operators compatible with this well-motivated formalism for physics above the electroweak scale, is allowed. (2) We present, for the first time, the complete angular distribution for $\bar{B} \to D^{(*)} \ell \bar{X}$ decays with a massive right-handed neutrino. (3) We address the $\langle \Delta A_{\rm FB} \rangle$ anomaly with the aid of a massive RH neutrino, and show that a massless RH neutrino fails to do so.

II. SMNEFT

Standard model effective field theory (SMEFT) [28–30] is defined in terms of $SU(3)_C \times SU(2)_L \times U(1)_Y$ invariant higher dimensional operators \mathcal{O}^i built from SM fields:

$$\mathcal{L} = \sum_{i} \frac{c_i}{\Lambda^{d_i - 4}} \mathcal{O}^i, \tag{1}$$

where Λ is the NP scale above the electroweak scale, $d_i > 4$ are integer dimensions of \mathcal{O}^i , and the dimensionless parameters c_i are the Wilson's coefficients (WCs) that can be calculated by matching the effective theory with the underlying theory.

Motivated by neutrino mass and oscillations, RH neutrinos that are sterile under the SM gauge interactions can be incorporated into SMEFT. The resulting EFT [31–35], called SMNEFT, includes additional interactions of the RH neutrinos with SM fields. The mass scale of the RH neutrino can vary over a large range. We consider the case

TABLE I. The origin of low-energy effective operators from SMNEFT. The last four operators in the second row arise by extending SMEFT to SMNEFT.

$\overline{\mathcal{O}_{\ell q}^{(3)}}$	$\mathcal{O}^{(1)}_{\ell equ}$	$\mathcal{O}_{\ell edq}$	$\mathcal{O}^{(3)}_{\ell eqd}$	\mathcal{O}_{nedu}	$\mathcal{O}_{\ell nuq}$	$\mathcal{O}^{(1)}_{\ell nqd}$	$\mathcal{O}_{\ell nqd}^{(3)}$
\mathcal{O}^{V}_{LL}	\mathcal{O}_{LL}^{S}	\mathcal{O}_{RL}^S	\mathcal{O}_{LL}^T	\mathcal{O}^V_{RR}	\mathcal{O}_{LR}^S	\mathcal{O}_{RR}^{S}	\mathcal{O}_{RR}^T

of a light RH neutrino so that it appears as an explicit degree of freedom in the EFT framework.

III.
$$\bar{B} \to D^{(*)} \mathcal{L} \bar{X}$$

In a general EFT at the m_b scale, NP in semileptonic B decays can be described by four-fermion contact interactions that give $b \to c\ell\bar{X}$. The dimension-six $SU(3)_C \times U(1)_Q$ invariant Lagrangian is

$$-\mathcal{L}_{\text{eff}} = \frac{4G_F V_{cb}}{\sqrt{2}} \left(\mathcal{O}_{LL}^V + \sum_{X=S,V,T \atop \alpha,\beta=L,R} C_{\alpha\beta}^X \mathcal{O}_{\alpha\beta}^X \right), \tag{2}$$

where

$$\mathcal{O}_{\alpha\beta}^{V} \equiv (\bar{c}\gamma^{\mu}P_{\alpha}b)(\bar{\ell}\gamma^{\mu}P_{\beta}\nu), \tag{3}$$

$$\mathcal{O}_{\alpha\beta}^{S} \equiv (\bar{c}P_{\alpha}b)(\bar{\ell}P_{\beta}\nu), \tag{4}$$

$$\mathcal{O}_{\alpha\beta}^{T} \equiv \delta_{\alpha\beta} (\bar{c}\sigma^{\mu\nu}P_{\alpha}b)(\bar{\ell}\sigma_{\mu\nu}P_{\beta}\nu). \tag{5}$$

The first term in Eq. (2) is the SM contribution, and the NP is in the second term. As these operators should emerge from SMNEFT, the two EFTs must match at the electroweak scale. From SMEFT, only the operators \mathcal{O}_{LL}^V , \mathcal{O}_{LL}^S , \mathcal{O}_{RL}^{S} , and \mathcal{O}_{LL}^{T} arise, while SMNEFT yields four more operators: $\mathcal{O}^V_{RR},\,\mathcal{O}^S_{LR},\,\mathcal{O}^S_{RR},$ and $\mathcal{O}^T_{RR};$ see Table I. Note that \mathcal{O}_{LR}^V and \mathcal{O}_{RL}^V cannot be produced from the four-fermion operators in SMNEFT. The renormalization group running of the operators from Λ to m_Z and then down to the m_b scale has been discussed in Refs. [36,37]. The scalar operator $\mathcal{O}_{\ell nqd}^{(1)}$ and the tensor operator $\mathcal{O}_{\ell nqd}^{(3)}$ mix via the weak gauge couplings above the weak scale. Below the weak scale the operators \mathcal{O}_{RR}^{S} and \mathcal{O}_{RR}^{T} mix due to the electromagnetic interaction. The operators on the left and right side of the partition in Table I mix via Yukawa couplings. In what follows, we work in the low-energy effective field theory (LEFT) framework keeping in mind that the corresponding SMNEFT WCs can be obtained by carrying out the running and matching.

IV. FORMALISM

The differential decay distribution for $\bar{B} \to D\ell \bar{X}$ with a massless RH neutrino is given in Ref. [19]. We generalize the result for a nonzero RH neutrino mass m_N . A finite m_N affects both the phase space and the leptonic helicity

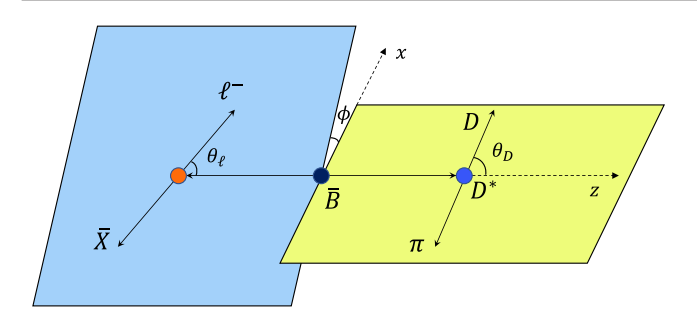


FIG. 1. Kinematic variables for $\bar{B} \to \ell^- \bar{N} D^* (\to D\pi)$.

amplitudes. For example, the operators with $\beta=R$ produce left-handed antineutrinos with helicity $\lambda_{\bar{N}}=\pm 1/2$ because the mass flips the helicity. The differential decay distribution for $\bar{B}\to D\ell\bar{X}$ can be expressed in terms of the three $\mathcal J$ functions as

$$\frac{d^2\Gamma_D}{dq^2d\cos\theta_\ell} = \sum_{i=0}^2 \mathcal{J}_i(q^2, \vec{\mathbf{C}}, m_N)\tilde{f}_i(\cos\theta_\ell), \quad (6)$$

where $q^2 \equiv (p_\ell + p_{\bar{N}})^2$ and $\tilde{f}_i(\cos\theta_\ell)$ are the angular functions with θ_ℓ the angle between the charged lepton momentum in the $\ell \bar{X}$ rest frame and the direction of the D momentum in the \bar{B} rest frame. The \mathcal{J}_i functions depend on q^2 , WCs $\vec{\mathbf{C}}$ and m_N , and are provided in the Supplemental Material [38]. Similarly, the differential decay distribution for $\bar{B} \to D^*(\to D\pi)\ell \bar{X}$ with nonzero m_N , can be written in terms of the 12 different angular structures that appear in the massless RH neutrino case:

$$\frac{d^4\Gamma_{D^*}}{dq^2d\cos\theta_{\ell}d\cos\theta_{D}d\phi} = \frac{3}{8\pi}\sum_{i}\mathcal{I}_{i}f_{i}(\cos\theta_{\ell},\cos\theta_{D},\phi),$$

where $\mathcal{I}_i \equiv \mathcal{I}_i(q^2, \vec{\mathbf{C}}, m_N)$, and the three angles are defined in Fig. 1; our convention for θ_ℓ differs from that often used by experimentalists [24]. For the complete expression see Supplemental Material [38]. For $m_N = 0$, our \mathcal{I} and \mathcal{J} functions match the I and J functions of Ref. [19]. We adopt the hadronic form factors of Ref. [39] including the corrections up to $1/m_c^2$ in the heavy-quark limit.

V. PHENOMENOLOGY

The general angular distributions can be integrated over subsets of the variables to construct several distributions. The differential distributions with respect to q^2 are

$$\Gamma_f^D(q^2) \equiv \frac{d\Gamma_D}{dq^2} = 2\mathcal{J}_0(q^2) + \frac{2}{3}\mathcal{J}_2(q^2),$$
(8)

$$\Gamma_f^{D^*}(q^2) \equiv \frac{d\Gamma_{D^*}}{dq^2} = 2\mathcal{I}_{1s}(q^2) + \mathcal{I}_{1c}(q^2) - \frac{1}{3}(2\mathcal{I}_{2s}(q^2) + \mathcal{I}_{2c}(q^2)). \tag{9}$$

We define 9 bins of the normalized q^2 -distributions [26],

$$\Delta x_i^{D^{(*)}} \equiv \frac{1}{\Gamma_{\text{tot}}^{D^{(*)}}} \int_{q_{i-1}^2}^{q_i^2} dq^2 \Gamma_f^{D^{(*)}}(q^2), \quad i = 2 \text{ to } 10, \quad (10)$$

where $\Gamma^{D^{(*)}}_{\text{tot}}$ is the total decay width after integrating $\Gamma^{D^{(*)}}_f(q^2)$ over the entire range of q^2 . The q^2 bins are defined by

$$q_i^2 \equiv m_B^2 + m_{D^{(*)}}^2 - 2m_B m_{D^{(*)}} \omega_i, \quad i = 1 \text{ to } 10,$$
 (11)

with $\omega_i = 1 + i/20$. The differential distributions with respect to $\cos \theta_\ell$, $\cos \theta_D$, and ϕ after integrating over the other variables, can be written in terms of five angular observables $\langle A_{FB}^{D^*} \rangle$, $\langle \tilde{F}_L \rangle$, $\langle F_L \rangle$, $\langle F_A \rangle$, and $\langle S_9 \rangle$:

$$\frac{1}{\Gamma_{\text{tot}}^{D^*}} \frac{d\Gamma^{D^*}}{d\cos\theta_{\ell}} = \frac{1}{2} - \langle A_{\text{FB}}^{D^*} \rangle \cos\theta_{\ell} + \frac{1}{4} (1 - 3\langle \tilde{F}_L \rangle) \frac{3\cos^2\theta_{\ell} - 1}{2}, \quad (12)$$

$$\frac{1}{\Gamma_{\text{tot}}^{D^*}} \frac{d\Gamma^{D^*}}{d\cos\theta_D} = \frac{3}{4} \left[1 - \langle F_L \rangle + (3\langle F_L \rangle - 1)\cos^2\theta_D \right], \quad (13)$$

$$\frac{1}{\Gamma_{\text{tot}}^{D^*}} \frac{d\Gamma^{D^*}}{d\phi} = \frac{1}{2\pi} + \frac{2}{3\pi} \langle S_3 \rangle \cos(2\phi)
+ \frac{2}{3\pi} \langle S_9 \rangle \sin(2\phi),$$
(14)

where the q^2 -averaged observables are defined by

$$\langle O \rangle \equiv \frac{1}{\Gamma_{\text{tot}}^{D^{(*)}}} \int_{q_{\text{int}}^2}^{q_{\text{max}}^2} dq^2 O(q^2) \Gamma_f^{D^{(*)}}(q^2).$$
 (15)

The values of $\langle A_{\rm FB}^{D^*} \rangle$, $\langle \tilde{F}_L \rangle$, $\langle F_L \rangle$, and $\langle S_3 \rangle$, measured by the Belle experiment are listed in Table II. Measurements of the two ratios of branching fractions $R_{D^{(*)}}^{\mu/e}$ are also listed in Table II. Several additional q^2 dependent angular asymmetries can be extracted from the full angular distribution through asymmetric integrals:

$$S_{4}(q^{2}) = \frac{3\pi}{8} \left(\int_{0}^{1} - \int_{-1}^{0} d \cos \theta_{\ell} d \cos$$

TABLE II. Ten observables that are sensitive to NP in the μ sector. The corresponding predictions for the three BPs of Table III are provided.

Observable	Measurement	BP1	BP2	BP3
$\Delta \langle A_{ m FB}^{D^*} angle$	0.0349 ± 0.0089	0.0188	-0.0014	-0.0016
$\Delta \langle F_L \rangle$	-0.0065 ± 0.0059	-0.0057	-0.0063	-0.0025
$\Delta \langle ilde{F}_L angle$	-0.0107 ± 0.0142	-0.0314	-0.0099	-0.0034
$\Delta \langle S_3 \rangle$	-0.0127 ± 0.0109	0.0035	0.0049	0.0007
$R_{D}^{\mu/e}$	$0.995 \pm 0.022 \pm 0.03$	9 1.015	1.036	1.012
$R_{D^*}^{\overline{\mu}/e}$	$0.99 \pm 0.01 \pm 0.03$	0.983	1.021	0.991
$\Delta x_2^{D^*}$	-0.0040 ± 0.0029	-0.0153	-0.0022	-0.0002
$\Delta x_3^{D^*}$	-0.0025 ± 0.0033	0.0	-0.0022	0.0001
$\Delta x_4^{D^*}$ $\Delta x_5^{D^*}$ $\Delta x_6^{D^*}$	0.0024 ± 0.0038	0.0014	-0.0022	0.0002
$\Delta x_5^{D^*}$	0.0043 ± 0.0046	0.0022	-0.0006	0.0002
$\Delta x_6^{D^*}$	-0.0035 ± 0.0052	0.0027	0.0009	0.0003
$\Delta x_7^{D^*}$	0.0066 ± 0.0056	0.0030	0.0018	0.0003
$\Delta x_8^{D^*} \\ \Delta x_9^{D^*}$	-0.0103 ± 0.0054	0.0032	0.0021	0.0003
$\Delta x_9^{D^*}$	0.0 ± 0.0052	0.0031	0.0020	0.0003
$\Delta x_{10}^{D^*}$	0.0019 ± 0.0044	0.0028	0.0017	0.0003
$\Delta \langle A_{ m FB}^D angle$		0.0401	-0.0032	-0.0209
$\Delta \langle S_4 angle$	• • •	0.0121	0.0087	0.0021
$\Delta \langle S_5 \rangle$	•••	-0.0128	-0.0051	0.0015

$$S_{5}(q^{2}) = \int_{-1}^{1} d\cos\theta_{\ell} \left(\int_{0}^{1} - \int_{-1}^{0} \right) \times d\cos\theta_{D} \left(\int_{0}^{\frac{\pi}{2}} - \int_{\frac{\pi}{2}}^{\pi} - \int_{\pi}^{\frac{3\pi}{2}} - \int_{\frac{3\pi}{2}}^{2\pi} \right) \times d\phi \frac{d^{4}\Gamma_{D^{*}}}{dq^{2}d\cos\theta_{\ell}d\cos\theta_{D}d\phi},$$
(17)

$$S_{7}(q^{2}) = \int_{-1}^{1} d\cos\theta_{\ell} \left(\int_{0}^{1} - \int_{-1}^{0} \right)$$

$$\times d\cos\theta_{D} \left(\int_{0}^{\pi} - \int_{\pi}^{2\pi} \right)$$

$$\times d\phi \frac{d^{4}\Gamma_{D^{*}}}{dq^{2}d\cos\theta_{\ell}d\cos\theta_{D}d\phi}, \tag{18}$$

$$S_8(q^2) = \frac{3\pi}{8} \left(\int_0^1 - \int_{-1}^0 d\cos\theta_{\ell} \left(\int_0^1 - \int_{-1}^0 \right) \right)$$

$$\times d\cos\theta_D \left(\int_0^{\pi} - \int_{\pi}^{2\pi} \right)$$

$$\times d\phi \frac{d^4\Gamma_{D^*}}{dq^2 d\cos\theta_{\ell} d\cos\theta_D d\phi}.$$
(19)

In terms of the \mathcal{I} and \mathcal{J} functions,

$$A_{FB}^{D}(q^2) = -\frac{\mathcal{J}_1(q^2)}{\Gamma_f^{D}(q^2)},$$
 (20)

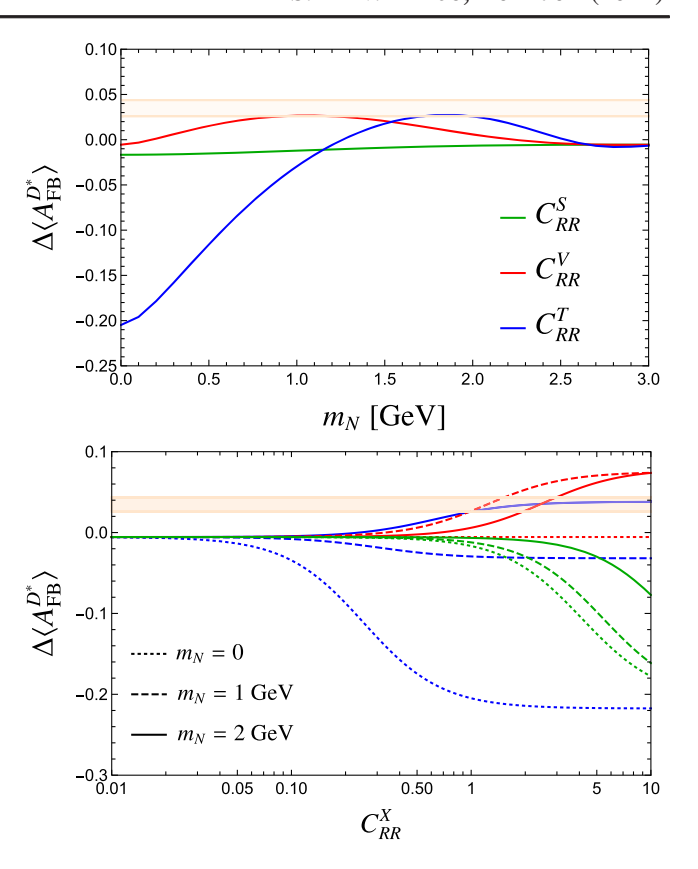


FIG. 2. Upper panel: $\Delta \langle A_{\rm FB}^{D^*} \rangle$ as a function of m_N for $C_{RR}^S = C_{RR}^V = C_{RR}^T = 1$. Lower panel: $\Delta \langle A_{\rm FB}^{D^*} \rangle$ as a function of C_{RR}^S (green), C_{RR}^V (red), and C_{RR}^T (blue) for $m_N = 0$ (dotted), 1 GeV (dashed), and 2 GeV (solid). The light orange band shows the Belle measurement at 1σ .

$$A_{FB}^{D^*}(q^2) = -\frac{\mathcal{I}_{6s}(q^2) + \frac{1}{2}\mathcal{I}_{6c}(q^2)}{\Gamma_f^{D^*}(q^2)},\tag{21}$$

$$F_L(q^2) = \frac{\mathcal{I}_{1c}(q^2) - \frac{1}{3}\mathcal{I}_{2c}(q^2)}{\Gamma_f^{D^*}(q^2)},\tag{22}$$

$$\tilde{F}_L(q^2) = \frac{1}{3} - \frac{8}{9} \frac{2\mathcal{I}_{2s}(q^2) + \mathcal{I}_{2c}(q^2)}{\Gamma_f^{D^*}(q^2)},\tag{23}$$

$$S_i(q^2) = \frac{\mathcal{I}_i(q^2)}{\Gamma_f^{D^*}(q^2)}, \quad i = \{3, 4, 5, 7, 8, 9\}.$$
 (24)

We find that the nonzero RH neutrino mass produces significant effects in the angular observables which may explain the 4σ tension in $\Delta\langle A_{\rm FB}^{D^*}\rangle$. In the upper panel of Fig. 2, we show $\Delta\langle A_{\rm FB}^{D^*}\rangle$ as a function m_N for $C_{RR}^S=C_{RR}^V=C_{RR}^T=1$. Clearly, a GeV RH neutrino with vector or tensor interactions can fit the $\Delta\langle A_{\rm FB}^{D^*}\rangle$ measurement within 1σ . In the lower panel of Fig. 2, we show the dependence of $\Delta\langle A_{\rm FB}^{D^*}\rangle$ on the LEFT WCs for three values of m_N , taking only one of the WCs to be nonzero at a time. We observe that if the RH neutrino is massless (dotted curves), $\Delta\langle A_{\rm FB}^{D^*}\rangle$

TABLE III. The parameters for three benchmark points. The WCs not listed are zero.

	m_N (GeV)	C_{RR}^V	C_{RR}^S	C_{RR}^{T}	C_{LL}^V	C_{LL}^S	C_{LL}^{T}
BP1	0.4	0.82	0.1	0.02	-0.4	0	0
BP2	1.6	0.15	-0.3	0.06	0	0	0
BP3	0	0	0	0	0	0.06	0.02

is always below the SM prediction. However, for $m_N=1$ GeV, the $\Delta\langle A_{\rm FB}^{D^*}\rangle$ anomaly can be explained if $C_{RR}^V\approx 1$ (red dashed curve). For $m_N=2$ GeV, the anomaly can be explained by both $C_{RR}^V\approx 2$ and $C_{RR}^T\approx 1$. However, these illustrative scenarios are excluded by other measurements in Table II. So, to reproduce the $\Delta\langle A_{\rm FB}^{D^*}\rangle$ anomaly and the other measurements in Table III, we choose three benchmark points (BPs) of Table III. BP1 has both LH and RH interactions, while BP2 and BP3 only have RH and LH interactions, respectively. The predictions for the three BPs for the 15 measurements are provided in Table II and Fig. 3. Since there is no interference between LH and RH contributions, scenarios with only RH interactions (like BP2) necessarily increase $R_D^{\mu/e}$ and $R_D^{\mu/e}$, and it is not possible to sufficiently enhance $\Delta\langle A_{\rm FB}^{D^*}\rangle$. Only LH interactions (BP3) are unable to adequately reproduce all the measurements. It is clear that BP1 can alleviate the tension in $\Delta\langle A_{\rm FB}^{D^*}\rangle$ to within $\sim 2\sigma$. This requires a large correction to

the vector LH interaction in conjunction with a large contribution from the vector RH neutrino interaction. It is possible to obtain predictions closer to the central values of $\Delta \langle A_{\rm FB}^{D^*} \rangle$ and $\Delta \tilde{F}_L$, at the expense of an even larger cancellation of C_{LL}^V with the SM. One such set of parameters is $C_{LL}^V = -0.84$, $C_{RR}^V = 1.0$, $C_{RR}^S = 0.05$, $C_{RR}^T = 0.03$, and $m_N = 0.3$ GeV.

We now calculate $A_{FB}^{D^*}(q^2)$, $\tilde{F}_L(q^2)$, $F_L(q^2)$, and $S_3(q^2)$ for our BP scenarios. The binned observables are defined by

$$O_i \equiv \frac{1}{\Gamma_{\text{tot}}^{D^{(*)}}} \int_{q_{i-1}^2}^{q_i^2} dq^2 O(q^2) \Gamma_f^{D^{(*)}}(q^2), \quad i = 2 \text{ to } 10.$$
 (25)

We present the four binned angular observables for the three BPs in Fig. 3. We also show the normalized q^2 distribution for $\bar{B} \to D\ell \bar{X}$. Large deviations from the SM are evident in several q^2 bins. The error bars in the middle and lower panels indicate the uncertainties due to the hadronic form factors. We estimate these as the range of predictions using our chosen form factors [39] and the form factors of Refs. [40,41]. We see that ΔS_3 is quite sensitive to the form factor.

Other observables that have not yet been measured and can be significantly modified by NP include the forward-backward asymmetry in $\bar{B} \to D\ell \bar{X}$, $A_{\rm FB}^D$. In the SM, this is suppressed by m_{ℓ}^2 . In the limit $m_{\ell} \to 0$, $A_{\rm FB}^D$ is proportional

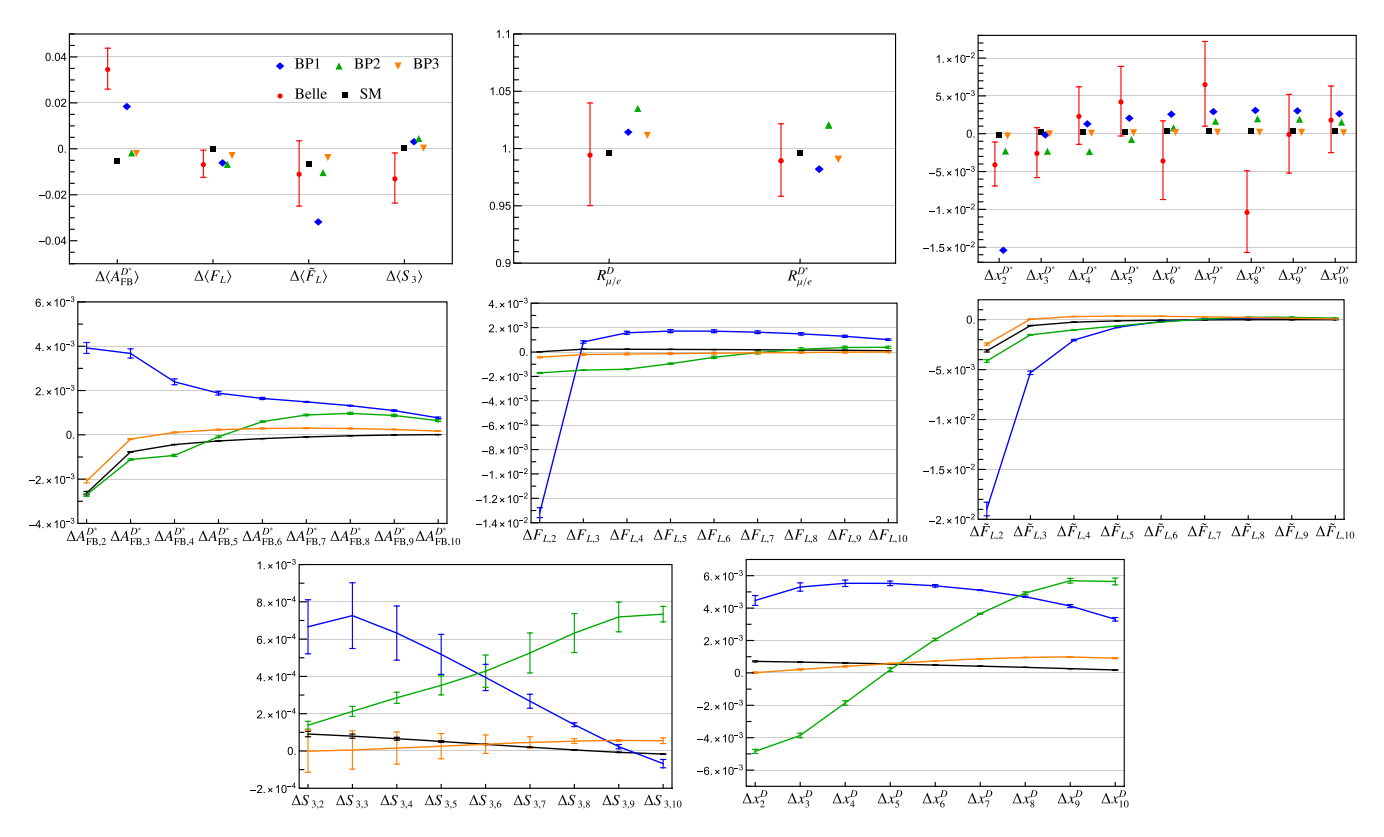


FIG. 3. The expectations for the SM and three BPs for the observables in the upper and middle panels of Table II. The Belle measurements are shown in the upper panels. The error bars in the middle and lower panels are hadronic form factor uncertainties.

FIG. 4. q^2 distributions of the three angular observables in the lower panel of Table II.

to q^2 with the new LH interactions $(\mathcal{O}_{LL}^S + \mathcal{O}_{RL}^S)\mathcal{O}_{LL}^T$. With the new RH interactions $(\mathcal{O}_{LR}^V + \mathcal{O}_{RR}^V)^2$, $A_{\rm FB}^D$ is proportional to $m_N^2(1-m_N^2/q^2)$, and for $(\mathcal{O}_{LR}^S + \mathcal{O}_{RR}^S)\mathcal{O}_{RR}^T$, it is proportional to $q^2(1-m_N^2/q^2)$. The q^2 averaged values of $\Delta A_{\rm FB}^D$, ΔS_4 and ΔS_5 for the BPs are displayed in Table II. In Fig. 4, we plot the corresponding q^2 binned observables and find that large deviations from the SM are possible.

VI. SUMMARY

We have presented the angular distributions for $\bar{B} \to D\ell\bar{X}$ and $\bar{B} \to D^*\ell\bar{X} \to D\pi\ell\bar{X}$, where X may be a massive RH neutrino, for the most general set of operators in LEFT; see section IV of Supplemental Material [38] for complete expressions. Interestingly, compared to the massless RH neutrino case, no new angular structures result. However,

to obtain a positive value of $\Delta \langle A_{\rm FB}^{D^*} \rangle$, as suggested by Belle data, a nonzero m_N is needed if the new physics only affects the muon sector. We also made predictions for several angular observables that differ substantially from SM expectations.

ACKNOWLEDGMENTS

We thank P. Urquijo for a useful discussion. A. D. is supported in part by the U.S. National Science Foundation under Grant No. PHY-1915142. H. L. is supported by ISF, BSF and Azrieli foundation. D. M. is supported in part by the U.S. Department of Energy under Grant No. desc0010504. D. M. thanks KITP, Santa Barbara for its hospitality, and support via the NSF under Grant No. PHY-1748958, during the completion of this work.

^[1] J. P. Lees *et al.* (*BABAR* Collaboration), Phys. Rev. Lett. **109**, 101802 (2012).

^[2] J. P. Lees *et al.* (*BABAR* Collaboration), Phys. Rev. D 88, 072012 (2013).

^[3] R. Aaij *et al.* (LHCb Collaboration), Phys. Rev. Lett. **115**, 111803 (2015); **115**, 159901(E) (2015).

^[4] M. Huschle *et al.* (Belle Collaboration), Phys. Rev. D 92, 072014 (2015).

^[5] Y. Sato *et al.* (Belle Collaboration), Phys. Rev. D **94**, 072007 (2016).

^[6] S. Hirose *et al.* (Belle Collaboration), Phys. Rev. Lett. 118, 211801 (2017).

^[7] R. Aaij *et al.* (LHCb Collaboration), Phys. Rev. Lett. **120**, 171802 (2018).

^[8] S. Hirose *et al.* (Belle Collaboration), Phys. Rev. D **97**, 012004 (2018).

^[9] R. Aaij *et al.* (LHCb Collaboration), Phys. Rev. D 97, 072013 (2018).

^[10] A. Abdesselam et al. (Belle Collaboration), arXiv: 1904.08794.

^[11] Y. S. Amhis *et al.* (HFLAV Collaboration), Eur. Phys. J. C 81, 226 (2021).

^[12] R. Aaij *et al.* (LHCb Collaboration), Phys. Rev. Lett. **120**, 121801 (2018).

^[13] R. Watanabe, Phys. Lett. B 776, 5 (2018).

^[14] X.-G. He and G. Valencia, Phys. Rev. D 87, 014014 (2013).

^[15] G. Cvetič, F. Halzen, C. S. Kim, and S. Oh, Chin. Phys. C 41, 113102 (2017).

^[16] P. Asadi, M. R. Buckley, and D. Shih, J. High Energy Phys. 09 (2018) 010.

^[17] A. Greljo, D. J. Robinson, B. Shakya, and J. Zupan, J. High Energy Phys. 09 (2018) 169.

^[18] K. S. Babu, B. Dutta, and R. N. Mohapatra, J. High Energy Phys. 01 (2019) 168.

^[19] R. Mandal, C. Murgui, A. Peñuelas, and A. Pich, J. High Energy Phys. 08 (2020) 022.

^[20] B. Abi et al. (Muon g-2 Collaboration), Phys. Rev. Lett. 126, 141801 (2021).

^[21] R. Aaij et al. (LHCb Collaboration), Nat. Phys. 18, 277 (2022).

^[22] M. Duraisamy and A. Datta, J. High Energy Phys. 09 (2013) 059.

^[23] M. Duraisamy, P. Sharma, and A. Datta, Phys. Rev. D 90, 074013 (2014).

^[24] B. Bhattacharya, T. Browder, Q. Campagna, A. Datta, S. Dubey, L. Mukherjee, and A. Sibidanov, in *2022 Snowmass Summer Study* (2022), arXiv:2203.07189.

^[25] E. Waheed *et al.* (Belle Collaboration), Phys. Rev. D **100**, 052007 (2019); **103**, 079901(E) (2021).

- [26] C. Bobeth, D. van Dyk, M. Bordone, M. Jung, and N. Gubernari, Eur. Phys. J. C 81, 984 (2021).
- [27] A. Carvunis, A. Crivellin, D. Guadagnoli, and S. Gangal, Phys. Rev. D 105, L031701 (2022).
- [28] B. Grzadkowski, M. Iskrzynski, M. Misiak, and J. Rosiek, J. High Energy Phys. 10 (2010) 085.
- [29] B. Henning, X. Lu, and H. Murayama, J. High Energy Phys. 01 (2016) 023.
- [30] I. Brivio and M. Trott, Phys. Rep. 793, 1 (2019).
- [31] F. del Aguila, S. Bar-Shalom, A. Soni, and J. Wudka, Phys. Lett. B 670, 399 (2009).
- [32] A. Aparici, K. Kim, A. Santamaria, and J. Wudka, Phys. Rev. D 80, 013010 (2009).
- [33] S. Bhattacharya and J. Wudka, Phys. Rev. D **94**, 055022 (2016); **95**, 039904(E) (2017).
- [34] Y. Liao and X.-D. Ma, Phys. Rev. D 96, 015012 (2017).

- [35] I. Bischer and W. Rodejohann, Nucl. Phys. **B947**, 114746 (2019).
- [36] A. Datta, J. Kumar, H. Liu, and D. Marfatia, J. High Energy Phys. 02 (2021) 015.
- [37] A. Datta, J. Kumar, H. Liu, and D. Marfatia, J. High Energy Phys. 05 (2021) 037.
- [38] Please see Supplemental Material at http://link.aps.org/supplemental/10.1103/PhysRevD.106.L011702 for complete expressions for the angular distributions.
- [39] M. Bordone, N. Gubernari, D. van Dyk, and M. Jung, Eur. Phys. J. C 80, 347 (2020).
- [40] M. Tanaka and R. Watanabe, Phys. Rev. D 87, 034028 (2013).
- [41] S. Iguro and R. Watanabe, J. High Energy Phys. 08 (2020) 006.